NAVAL POSTGRADUATE SCHOOL

MONTEREY, CALIFORNIA

THESIS

NONLINEAR FEEDBACK CONTROL OF THE ROTARY INVERTED PENDULUM

by

Ellen M. Bradford

June 2017

Thesis Advisor: Xiaoping Yun
Co-Advisor: James Calusdian

Approved for public release. Distribution is unlimited.

THIS PAGE INTENTIONALLY LEFT BLANK

REPORT DOCUMENTATION PAGE			*Form Approved OMB No. 0704–0188*
Public reporting burden for this collection of information is estimated to average 1 hour per response, including the time for reviewing instruction, searching existing data sources, gathering and maintaining the data needed, and completing and reviewing the collection of information. Send comments regarding this burden estimate or any other aspect of this collection of information, including suggestions for reducing this burden, to Washington headquarters Services, Directorate for Information Operations and Reports, 1215 Jefferson Davis Highway, Suite 1204, Arlington, VA 22202-4302, and to the Office of Management and Budget, Paperwork Reduction Project (0704-0188) Washington, DC 20503.			
1. AGENCY USE ONLY ***(Leave blank)***	**2. REPORT DATE** June 2017	**3. REPORT TYPE AND DATES COVERED** Master's thesis	
4. TITLE AND SUBTITLE NONLINEAR FEEDBACK CONTROL OF THE ROTARY INVERTED PENDULUM			**5. FUNDING NUMBERS**
6. AUTHOR(S) Ellen M. Bradford			
7. PERFORMING ORGANIZATION NAME(S) AND ADDRESS(ES) Naval Postgraduate School Monterey, CA 93943-5000			**8. PERFORMING ORGANIZATION REPORT NUMBER**
9. SPONSORING /MONITORING AGENCY NAME(S) AND ADDRESS(ES) N/A			**10. SPONSORING / MONITORING AGENCY REPORT NUMBER**
11. SUPPLEMENTARY NOTES The views expressed in this thesis are those of the author and do not reflect the official policy or position of the Department of Defense or the U.S. Government. IRB Protocol number ____N/A____.			
12a. DISTRIBUTION / AVAILABILITY STATEMENT Approved for public release. Distribution is unlimited.			**12b. DISTRIBUTION CODE**

13. ABSTRACT (maximum 200 words)

The inverted pendulum, a popular problem of study, is presented in many textbooks as a nonminimum phase system. The majority of control algorithms for this problem include linearizing the system about a fixed operating point. In this thesis, a nonlinear form of control is considered.

A model for the rotary inverted pendulum system was derived and validated by comparing simulations using the derived equations to experimental data. The system parameters were tuned until the simulation and experimental data fit. A feedback linearization controller was then designed based on the model derived. The simulated implementation of the feedback linearization was successful but indicated continuous motion of the system. The experimental results of the feedback linearization controller were less successful than simulations. The simulated results also indicated unstable zero dynamics of the system, which were characterized and confirmed to be unstable. Finally, an intuitive fix was applied to add terms to the feedback linearization controller to account for the zero dynamics. The results of this controller in simulation were successful but did not produce a substantially different response in the experimental system

14. SUBJECT TERMS inverted pendulum, nonlinear feedback, zero dynamics			**15. NUMBER OF PAGES** 61
			16. PRICE CODE
17. SECURITY CLASSIFICATION OF REPORT Unclassified	**18. SECURITY CLASSIFICATION OF THIS PAGE** Unclassified	**19. SECURITY CLASSIFICATION OF ABSTRACT** Unclassified	**20. LIMITATION OF ABSTRACT** UU

NSN 7540–01-280-5500

Standard Form 298 (Rev. 2–89)
Prescribed by ANSI Std. 239–18

THIS PAGE INTENTIONALLY LEFT BLANK

Approved for public release. Distribution is unlimited.

NONLINEAR FEEDBACK CONTROL OF THE ROTARY INVERTED PENDULUM

Ellen M. Bradford
Ensign, United States Navy
B.S., United States Naval Academy, 2016

Submitted in partial fulfillment of the
requirements for the degree of

MASTER OF SCIENCE IN ELECTRICAL ENGINEERING

from the

NAVAL POSTGRADUATE SCHOOL
June 2017

Approved by: Xiaoping Yun
Thesis Advisor

James Calusdian
Co-Advisor

R. Clark Robertson
Chair, Department of Electrical and Computer Engineering

THIS PAGE INTENTIONALLY LEFT BLANK

ABSTRACT

The inverted pendulum, a popular problem of study, is presented in many textbooks as a nonminimum phase system. The majority of control algorithms for this problem include linearizing the system about a fixed operating point. In this thesis, a nonlinear form of control is considered.

A model for the rotary inverted pendulum system was derived and validated by comparing simulations using the derived equations to experimental data. The system parameters were tuned until the simulation and experimental data fit. A feedback linearization controller was then designed based on the model derived. The simulated implementation of the feedback linearization was successful but indicated continuous motion of the system. The experimental results of the feedback linearization controller were less successful than simulations. The simulated results also indicated unstable zero dynamics of the system, which were characterized and confirmed to be unstable. Finally, an intuitive fix was applied to add terms to the feedback linearization controller to account for the zero dynamics. The results of this controller in simulation were successful but did not produce a substantially different response in the experimental system.

THIS PAGE INTENTIONALLY LEFT BLANK

TABLE OF CONTENTS

THIS PAGE INTENTIONALLY LEFT BLANK

LIST OF FIGURES

LIST OF TABLES

THIS PAGE INTENTIONALLY LEFT BLANK

I. INTRODUCTION

A. BACKGROUND

The inverted pendulum is a common benchmark in control theory. It is a problem that can be easily visualized because everyone at one point has tried to balance a broomstick on his or her palm. While the broomstick is a rather unsophisticated experiment, it demonstrates the inherit instability of the inverted pendulum system. The classical controls laboratory problem consists of a rigid pendulum attached to a cart. The goal is to keep the pendulum inverted with the only input being the forward and backward force on the cart. This problem is also commonly adapted to a rotary system in which the cart is replaced by a rotary arm connected to a DC motor and the torque of the motor is the input. A schematic of the cart and pendulum, as well as the rotary pendulum system, is shown in Figure 1. The dynamic motion equation of a pendulum includes sine and cosine terms; therefore, the system is nonlinear. There are two equilibrium points of the pendulum. The first is its downward position, often called the stable equilibrium point. This is an asymptotically stable equilibrium, and any position aside from the inverted position converges to this point. The other equilibrium point exists in the inverted position, often called the unstable equilibrium point. No positions of the pendulum converge to this point. The inverted pendulum is an under-actuated system, meaning that there are more degrees of freedom than there are inputs. The inherent instability of the system, as well as its nonlinear nature, makes the inverted pendulum a popular problem of study in control systems engineering.

In many undergraduate controls courses, the inverted pendulum is stabilized using linearization of the equations of motion and pole placement. This technique, called state-feedback control, is reviewed in Chapter III. The basic steps of linearization are to obtain the nonlinear equations of motion of the system, linearize them about an operating point, usually the inverted position of the pendulum, then choose either a proportional integral (PI), proportional derivative (PD), or proportional integral derivative (PID) controller to stabilize the system. Linearization is a fairly simple technique for control of the inverted pendulum and works well in a laboratory environment; however, many real life systems are

more complex, affected by disturbances, and rarely function about only one operating point [1]. For these reasons, other nonlinear control techniques may be more appropriate.

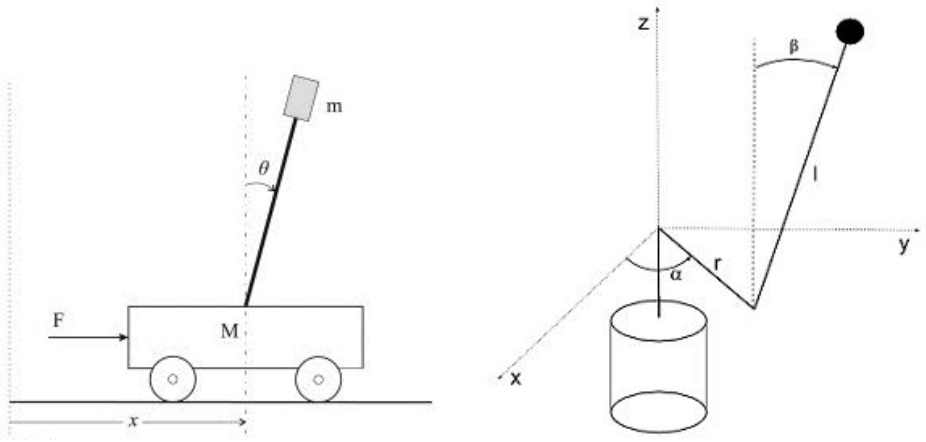

Figure 1. Schematics of the Linear and Rotary Inverted Pendulum Systems. Adapted from [2] and [3].

The focus of this thesis is to use feedback linearization to stabilize the rotary inverted pendulum. Feedback linearization is a form of control in which the input is used to linearize the system. Given a nonlinear model of a system, an input can be designed with two terms. The first is a nonlinear term that effectively cancels out the nonlinear behavior of the system. The second portion is a linear controller which works to stabilize the remaining linear portion of the system. Feedback linearization has advantages over linearized control because of the ability to operate over a wider range of motion than the small neighborhood of positions near the set operating point. For feedback linearization to be effective, a model of the system must be known. If unmodeled nonlinearities exist, then the system may become unstable. Additionally, according to Barbieri, Drakunov, and Grossimon feedback linearization control is known to be ineffective for controlling non-minimum phase systems [4]. These are systems that have unstable zero dynamics. The inverted pendulum system has unstable zero dynamics that are examined in this thesis. In order to compensate for the instability, additional terms are added to the linear portion of the controller.

B. MOTIVATION

While study into the inverted pendulum has been extensive, it is still a problem of interest. Prasad, Tyahi, and Om argue that most dynamic systems including robotic systems, missile systems, and industrial processes are nonlinear in nature [5]. The inverted pendulum is a somewhat simple stepping stone into the study and control of other more complex nonlinear systems. Applications of the inverted pendulum include wheeled mobile robots, which can be useful for personal mobility.

C. PRIOR WORK

There are nonlinear control techniques that have been successfully implemented on the inverted pendulum system. One common method is an input switching control method. In 1992, Wei performed a nonlinear switching control on an inverted pendulum on a cart [6]. The goal of the study was to create an algorithm that would both balance the pendulum on the cart while minimizing the linear motion of the cart. Control of the system was achieved in a set of five different cycles. Each cycle was defined by the pendulum angle and angular velocity and set a different value to the input. In each cycle, the pendulum overshot the straight-up position by continually smaller amounts. The control input was a piecewise function between three different values.

A more formal method of switching control is called sliding-mode control. Sliding-mode control switches between two inputs in order to drive the system toward a desired, pre-defined surface. Barbieri, Drakunov, and Grossimon explain that sliding-mode control is desirable for its robustness in systems where the dynamics are not fully known [4]. This surface is a linear combination of the states of the system. The sign of the input changes based on value of the surface. According to Khanesar, Teshnehlab, and Shoorehdeli [7], achieving sliding-mode control can be broken into two steps. The first is to select an appropriate sliding surface. The second is to ensure the input forces the system to converge to the sliding surface. Once the system converges to the surface, the surface itself determines the limitations of the system. To ensure that the system converges to the sliding surface, a Lyapunov function is defined to be a positive definite function of the surface.

Then, inputs are designed so that the time derivative of the Lyapunov function is negative, ensuring that both the Lyapunov function and sliding surface approach zero [7].

In 1996, Enrique Barbieri and Sergey Drakunov published a paper in which they used software to simulate sliding-mode controller on a rotary inverted pendulum system [4]. The goal of the study was to design a controller that could hold the pendulum at any commanded angle. They ran two simulations, one in which the pendulum was to be stable in the inverted position and another in which the pendulum was to be held at a 45 degree angle. The simulations showed that the pendulum could be stabilized in the inverted position after the rotary arm did the three full revolutions. The pendulum could be held at 45 degrees but required the rotary arm to spin continuously.

In 2007, Khanesar, Teshnehlab, and Shoorehdeli also published a paper investigating sliding-mode control of the rotary inverted pendulum system [7]. Noting that the position of the rotary arm could not be controlled if the angle of the pendulum was the only output, the authors designed two different sliding surfaces. One stabilized the rotary arm, and the other stabilized the pendulum. The Lyapunov function used was a linear combination of the two sliding surfaces, which weighted the stability of the pendulum over the stability of the rotary arm. A simulation was used to analyze the resulting controller. The pendulum was stabilized in its inverted position. The rotary arm settled at its desired position after the pendulum was stabilized.

Later in 2007, Khanesar and Shoorehdeli investigated combining sliding-mode control with fuzzy neural networks to stabilize the rotary inverted pendulum [1]. The same sliding surfaces and Lyapunov function was used as in his previous paper, but this time the dynamics of the rotary inverted pendulum system were left to be somewhat unknown. Fuzzy neural network is a layered control approach which is used to estimate unknown parameters through a series of trial runs. The combination of the fuzzy neural network with sliding-mode control stabilized the system with satisfactory results.

Among the applications of the inverted pendulum is a two wheeled robot. One mobile inverted pendulum robot was created by Grasser, D'Arrigo, Colombi, and Rufer to study the feasibility of the robot that could balance a driver on two coaxial wheels [8]. The resultant robot, called JOE, was about half a meter tall and weighed 12 kg. JOE was

designed only to study the problem, not to operate with a rider. The designers used two different linearized state space controllers to stabilize JOE. One controller balanced the pendulum, and the other controlled the position of the base of the robot. The robot was able to compensate for some disturbances in force; however, control was done via pole placement determined by system parameters unique to the system. If parameters of the system such as length or weight of the robot were changed, the control did not work.

In 2005, Pathak, Franch, and Agrawl published a paper about the dynamics of the two-wheeled inverted pendulum [9]. They studied the controllability properties of such a system and derived the partial feedback linearized form which led to a two-level velocity controller and a stabilizing position controller. Simulations of the control algorithms showed success; however, these controllers were again dependent on the parameters of the system and could not control a robot with different physical parameters.

In addition to parameter uncertainties, autonomous inverted pendulum systems are susceptible to changes in the terrain in which they operate. If used for personal transportation, the rider could feel uncomfortable and unsafe when climbing or descending a slope. In 2014, Dai, Gao, Jiang, Liu, and Li. modeled a two-wheeled inverted pendulum with an additional sliding joint at the top of the pendulum which could shift the weight of the load to keep the pendulum straight up when on a slope [10].

The work in mobile inverted pendulums can lead to more commercial robots for personal entertainment similar to the Segway. They may also offer an alternative to current motorized wheelchairs with the benefit of increased maneuverability.

D. THESIS ORGANIZATION

This thesis is organized into eight chapters. The setup of the experimental rotary pendulum system is included in Chapter II. Linearization and linear control of the inverted pendulum is designed, implemented, and analyzed in Chapter III. The inverted pendulum mathematical model is derived and validated in Chapter IV. Feedback linearization is derived, implemented, and analyzed in Chapter V. The zero dynamics of the system are derived in Chapter VI. Finally, in Chapter VII a linearized feedback controller is designed with added terms to account for the zero dynamics. Results, conclusions, and future work are discussed in Chapter VIII.

THIS PAGE INTENTIONALLY LEFT BLANK

II. EXPERIMENTAL SYSTEM

A. SYSTEM DESCRIPTION

All experiments were carried out on the Quanser Rotary Inverted Pendulum system, created by Quanser for educational purposes. The instructions for setup of the inverted pendulum system can be found in the Quanser manual [11]. The main hardware components are the pendulum system, data acquisition unit, and amplifier.

The rotary pendulum system consists of the SRV02 motor plant, a rotary arm, and the pendulum itself. A motor in the SRV02 plant is attached to a load gear shaft affixed to the flat rotary arm. The rotary arm has a metal shaft at the end able to rotate 360 degrees. Also on the rotary arm is an encoder to measure the angle of rotation of the metal shaft. The rigid pendulum is attached to the end of the metal shaft. The rotary pendulum system is shown in Figure 2.

Figure 2. Experimental Rotary Pendulum System. Source [11].

The motor of the plant is a Faulhaber Coreless DC motor model number 2338S006. The maximum input is +/-15.0 V. The maximum currents are 3.0 A peak or 1.0 A continuous. High-frequency signals may damage the brushes of this motor over time, so it is recommended by the manufacturer to limit the signal feedback to 50 Hz [12].

The potentiometer used in the SRV02 plant is a Vishay Spectrol model 132. It is a single turn 10.0 kΩ potentiometer that ranges over 352 degrees. The output of the sensor is +/-5.0 V over the full range. The potentiometer gives absolute position, while an encoder offers only relative position from initialization position [12].

The potentiometer is used in conjunction with an encoder to accurately measure the position of the load shaft. The encoder used is the U.S. Digital S1 single-ended optical shaft encoder [13]. It has a resolution 4096 counts per rotation, meaning it can detect changes in the pendulum angle as small as 0.09 degrees. It is operated by a single 5.0 V DC source. The maximum shaft speed it can measure is 100 rpm. The same type of encoder is attached to the rotary arm to measure the angular position of the pendulum [13].

The tachometer is used to measure the speed of the load shaft. It is connected directly to the shaft of the DC motor to prevent a time lapse of the response and ensures that the motor speed is correctly measured [12].

A table of parameters associated with the SRV02 plant can be found in [12]. While these parameters are not listed in the user manual for the inverted pendulum system, some of them are used in the modelling of the pendulum system when adding actuation dynamics. For convenience, a table of parameters used in calculations is shown in Table 1.

The parameters for the inverted pendulum can be found in [11]. These parameters are used in the model derivation in Chapter IV. The list of parameters of the inverted pendulum are shown in Table 2.

Table 1. Relevant SRV02 Plant Parameters. Adapted from [12].

Symbol	Description	Value	Unit
$\mathbf{K_g}$	High gear total gear ratio	70	
$\mathbf{k_t}$	Motor current torque constant	$7.68 \cdot 10^{-3}$	Nm/A
$\mathbf{k_m}$	Motor back emf constant	$7.68 \cdot 10^{-3}$	V/(rad/s)
$\mathbf{n_m}$	Motor efficiency	0.69	
$\mathbf{n_g}$	Gearbox efficiency	0.9	
$\mathbf{R_m}$	Motor armature resistance	2.6	Ohms

Table 2. Rotary Pendulum System Parameters. Adapted from [11].

Symbol	Description	Value	Unit
$\mathbf{m_p}$	Mass of pendulum	0.127	kg
$\mathbf{L_p}$	Total length of pendulum	0.337	m
$\mathbf{l_p}$	Distance from pivot to center of mass of pendulum	0.156	m
$\mathbf{J_{p,cm}}$	Pendulum moment of inertia about center of mass	0.0012	$kg \cdot m^2$
$\mathbf{B_p}$	Pendulum viscous damping coefficient	0.0024	N·m·s/rad
$\mathbf{m_r}$	Mass of rotary arm	0.257	kg
$\mathbf{L_r}$	Rotary arm length pivot to tip	0.216	m
$\mathbf{l_r}$	Rotary arm distance pivot to center of mass	0.0619	m
$\mathbf{J_{arm,cm}}$	Rotary arm moment of inertia about its center of mass	$9.98 \cdot 10^{-4}$	$kg \cdot m^2$
$\mathbf{B_r}$	Rotary arm viscous damping coefficient	0.0024	N·m·s/rad
$\mathbf{J_{arm}}$	Rotary arm moment of inertia about pivot	0.002	$kg \cdot m^2$

The data acquisition unit used is the Quanser Q2-USB. The maximum closed loop control rate using this device is 2.0 kHz. A full list of specifications can be found in [14].

The power amplifier used, the VoltPAQ-X1, is a linear power amplifier able to output 24.0 V continuously and 4.16 A continuously. There are four analog inputs with a range between -10.0 V and 10.0 V. The full list of specifications is available [15].

B. SOFTWARE

All simulations were carried out using Simulink in Matlab 2015b. This version of Matlab was used because of the author's prior experience. The system and controller were initially represented as S-functions in Simulink. An S-function is a user defined script that interfaces with the Simulink engine to solve for outputs given inputs. The Quanser hardware is not compatible with S-functions, so after the simulation was working, the equations executed in the S-functions were rebuilt using Simulink Math Operation blocks. Building these equations with Math Operations was not difficult but required attention to detail in order to make sure all the correct operations took place. Simulation outputs using the Math Operations were compared to those using an S-function to check for correctness. After the math blocks were confirmed to work correctly, the simulation was sent to the experimental computer system via Google Drive.

The experiments were run using Simulink in Matlab 2014b. This earlier version of Matlab was used because it had already been installed on the system and was compatible with the Quanser hardware. Simulink was interfaced with the experimental hardware using QUARC Real-time Rapid Control Prototyping software. This software is used for many QUARC products. The role of this software is to bridge the gap between simulation time and real time. Simulations are only limited by the processing power of the computer. The computer can solve the equations that govern the system faster than sensors can gather data and faster than the dynamics of the system will respond; therefore, the behavior of the inverted pendulum system can be simulated much faster than it could be observed. The QUARC software slows the simulation to operate at the same speed as the experimental system [16].

III. LINEAR CONTROL

Linear control, a simple way to control the inverted pendulum, is studied in many undergraduate courses. For familiarization and initial system testing, linear control through pole placement was performed.

The dynamic equations of the inverted pendulum system include sine and cosine terms and are, therefore, nonlinear. The nonlinear model is examined in Chapter IV. The system can be linearized through a first order Taylor series approximation. The format of a linearized system in state-space format is:

$$\dot{x} = Ax + Bu \tag{1}$$

$$y = Cx + Du. \tag{2}$$

The state vector for the inverted pendulum system is

$$x = \begin{bmatrix} \theta \\ \alpha \\ \dot{\theta} \\ \dot{\alpha} \end{bmatrix}.$$

In this representation, the variable θ represents the angle of the rotary arm, and the variable α represents the angle of the pendulum. The dot convention represents the time derivative of the variable. The linearized model is presented in [11]. The state matrices are

$$A = \begin{bmatrix} 0 & 0 & 1 & 0 \\ 0 & 0 & 0 & 1 \\ 0 & 81.4033 & -45.8259 & -.9319 \\ 0 & 122.0545 & -44.0966 & -1.3972 \end{bmatrix}, \tag{3}$$

$$B = \begin{bmatrix} 0 \\ 0 \\ 83.4659 \\ 80.3162 \end{bmatrix}, \tag{4}$$

$$C = \begin{bmatrix} 1 & 0 & 0 & 0 \\ 0 & 1 & 0 & 0 \end{bmatrix}, \tag{5}$$

and

$$D = \begin{bmatrix} 0 \\ 0 \end{bmatrix}. \tag{6}$$

A system is said to be controllable, according to Ogata [17], if for any initial state, it can be brought to another state in a finite amount of time using an unconstrained input. Ogata explains that for the system to be controllable, the rank of the controllability matrix T must equal the number of states. The controllability matrix for this system is

$$T = \begin{bmatrix} B & AB & A^2B & A^3B \end{bmatrix}. \tag{7}$$

The system was checked for controllability. In the case of the rotary inverted pendulum, the rank of the controllability matrix is four; therefore, the system is controllable [17].

Because the system is controllable, it can be stabilized using pole placement. Poles are the eigenvalues of the matrix A and determine the behavior of the system. All the eigenvalues of stable systems have a negative real portion. Unstable systems have a pole that has a positive real portion. Systems with single poles at the origin or on the imaginary axis are marginally stable, but the system becomes unstable if any of those poles are repeated. The poles of the inverted pendulum can be found using

$$\det(sI - A) = 0 \tag{8}$$

where s is a variable and I is the identity matrix of the same dimension as the matrix A. The poles of the system are at -48.4156, -5.8644, 0, and 7.0569. The pole in the right half

plane indicates that the system is not stable. The goal of pole placement is to use an input of the form $u = Kx$ in order to shift the poles to the left half plane. In this controller, K is a 1×4 vector. By plugging the input u into Equation (1), we get the new state equation

$$\dot{x} = (A + BK)x \ . \tag{9}$$

The poles of the system after pole placement are the eigenvalues of the matrix (A+BK). The values of K can be changed to modify the eigenvalues of the matrix

$$(A+BK) = \begin{bmatrix} 0 & 0 & 1 & 0 \\ 0 & 0 & 0 & 1 \\ 83.4659k_1 & 81.4033+83.4659k_2 & -45.8259+83.4659k_3 & -.9319+83.4659k_4 \\ 80.3162k_1 & 122.0545+80.3162k_2 & 44.0966+80.3162k_3 & -1.3972+80.3162k_4 \end{bmatrix}. \tag{10}$$

In addition to determining stability, the eigenvalues are linked to the damping ratio ζ and natural frequency ω_n of the system. The damping ratio determines the transient response of the system. If ζ is less than 1.0, then the system is underdamped, and the transient response is oscillatory. If is greater than 1.0, the system is overdamped and approaches the steady-state value without oscillations. Ogata states that the natural frequency determines the frequency of the system when it is not damped [17].

Poles which are closer to the origin have a greater effect on the overall system response than those farther away from the origin. A standard rule in control systems is that the effect of poles greater than 10 times those poles located near the origin can be neglected. The set of equations used to calculate the dominant poles of the system is

$$p_{1,2} = -\zeta\omega_n \pm j\omega_n\sqrt{1-\zeta^2}. \tag{11}$$

A natural frequency of 4.0 and a damping ratio of 0.5 produces the dominant poles of the system at −2.0+3.464j and −2 −3.464j. The remaining two poles are chosen to be at −40 and −45 as to have negligible effect on the system. The Matlab command ‘place’ was used to calculate gains given the system A and B matrices and the desired poles. The required gain values to shift the poles to these locations are

$$K = \begin{bmatrix} -7.8917 & 37.8317 & -2.9850 & 3.6222 \end{bmatrix}. \qquad (12)$$

This controller was represented as a gain block and tested in Simulink. A picture of the simulation diagram is shown in Figure 3. The output is shown in Figure 4.

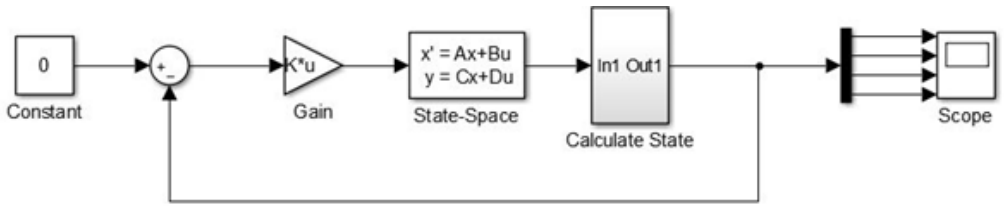

Figure 3. Simulink Diagram for Linear Control Simulations

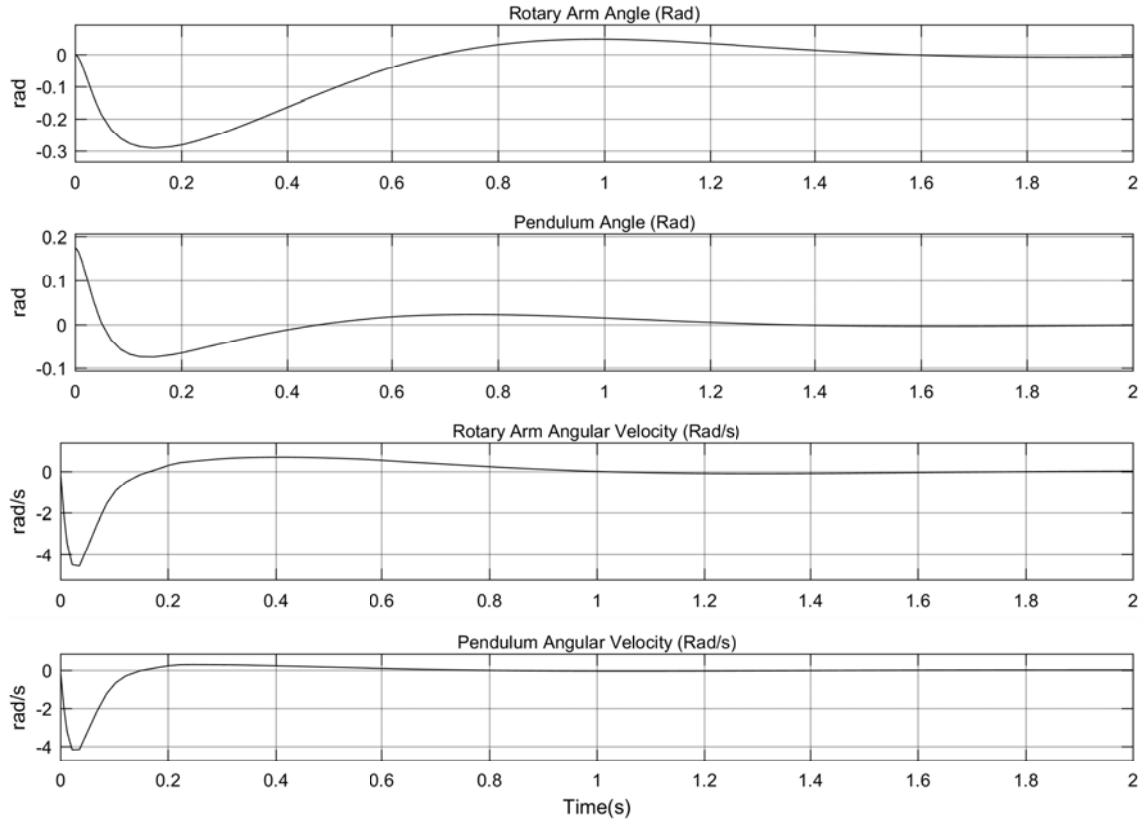

Figure 4. Underdamped Simulation Output

In the simulation, an initial pendulum angle of ten degrees from vertical was used. The pendulum and rotary arm both settle within two seconds of the start of the simulation. It is evident that the response is underdamped, as the pendulum angle oscillates before settling at zero. The same controller was then implemented on the experimental system. A picture of the Simulink diagram, interfaced with the experimental hardware, is shown in Figure 5. The green block titled SRV02-ET+ROTPEN-E interfaces with the actual input and output of the real rotary pendulum. The output of the states is shown in Figure 6. The experimental controller is only set to engage when the pendulum is within ten degrees of vertical to prevent the rotary arm from moving as the pendulum is manually brought to the desired starting position. During the first 1.5 s of the experiment, the pendulum was manually brought to its starting position. After that time, the controller engaged, and the pendulum was balanced by the system. In the experimental output, it is more difficult to notice the transient response because of the way the pendulum must be manually brought to the starting position.

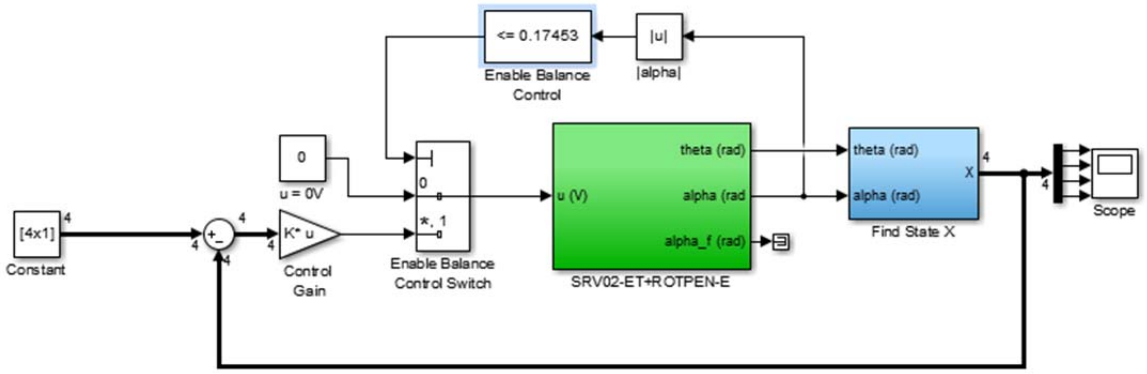

Figure 5. Simulation Diagram Interfaced with Hardware for Experiments

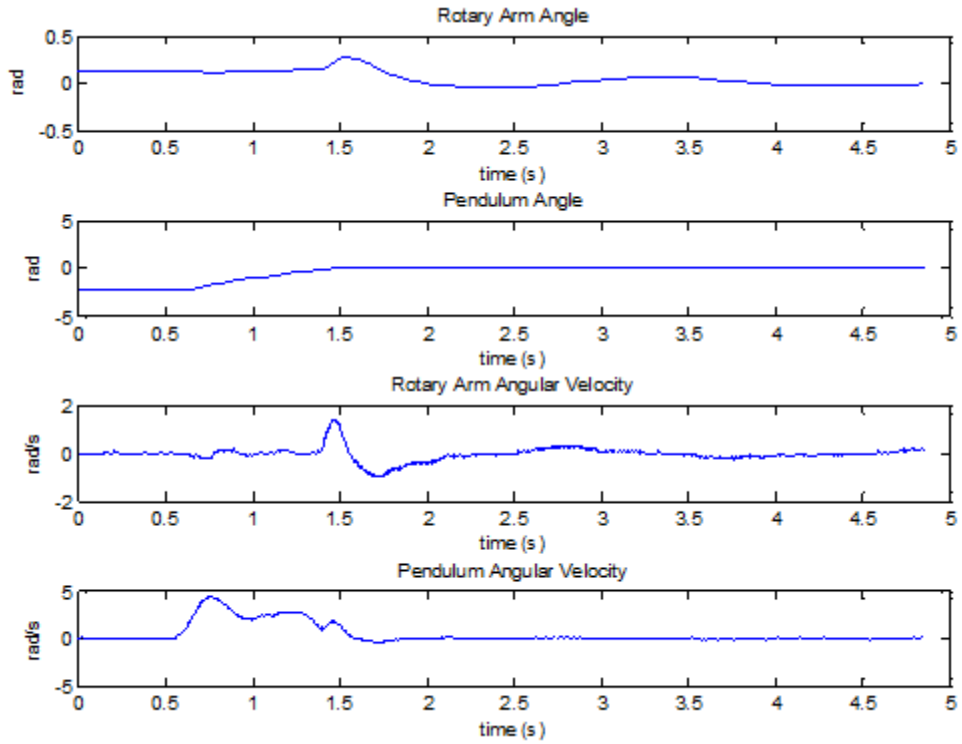

Figure 6. Experimental Output of Rotary Pendulum System Using Underdamped Pole Placement Method

In the first simulation and experiment, the poles were chosen to show an underdamped response. It is possible to recalculate the poles to show an overdamped response. The damping ratio was changed to 1.2. The dominant poles were calculated by using Equations (11) to be at −2.1467 and −7.4533. The remaining poles were left at –40 and –45. The new gain matrix is

$$K = \begin{bmatrix} -7.8917 & 45.1949 & -5.7471 & 6.5623 \end{bmatrix} . \qquad (13)$$

This controller was implemented in Simulink. The output of the states is shown in Figure 7. The pendulum and rotary arm settle at zero degrees much faster than when the system is underdamped. The pendulum still overshoots the final position but by a much smaller amount. The rotary arm does not oscillate around its final position. The new control gains were implemented on the experimental system. The output states are not

included, as there is not a large visual difference in the plots from the underdamped response experimentally.

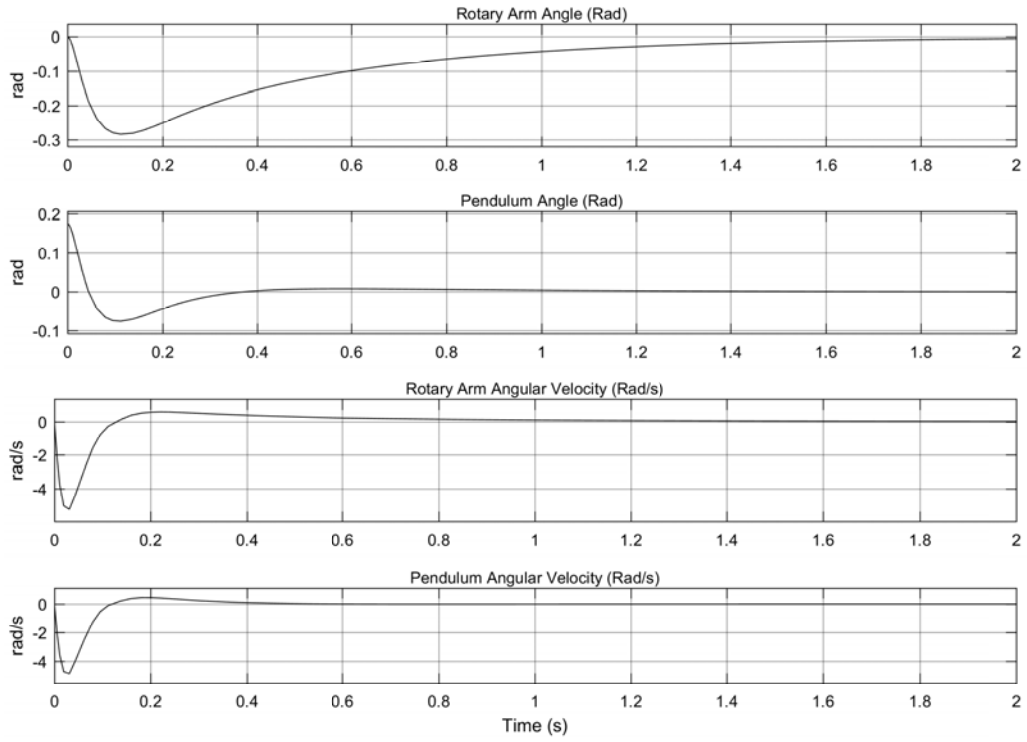

Figure 7. Output of Overdamped Simulation

THIS PAGE INTENTIONALLY LEFT BLANK

IV. MODEL DERIVATION AND VALIDATION

The inverted pendulum was studied through its linearized dynamic equations and pole placement in the previous chapter. The nonlinear model of the inverted pendulum is analyzed in this chapter. One requirement of linearization feedback control is to have an accurate model of the nonlinear system. The input of the system is designed to cancel out the nonlinearities of the system. If the model of the system is not accurate, the input will not account for all the dynamics of the system, and the controller will not perform as expected.

The mathematical model given in the Quanser manual was examined. If the model was accurate, then experimental data of the motion of the pendulum should match the output of the simulation given the same initial conditions. First, data was gathered from the experimental pendulum system, and then simulation data was gathered. The simulated and experimental data were then compared to assess the accuracy of the system's mathematical model.

The model of the pendulum system was represented as an S-function in Simulink. The experimental motion of the pendulum and the simulated motion of the pendulum using the equations of motion given in the user manual with a large initial angle are shown in Figure 8. The experimental and simulated pendulum motion with a small initial angle are shown in Figure 9. In these figures, the zero angle is defined as the pendulum's stable equilibrium point.

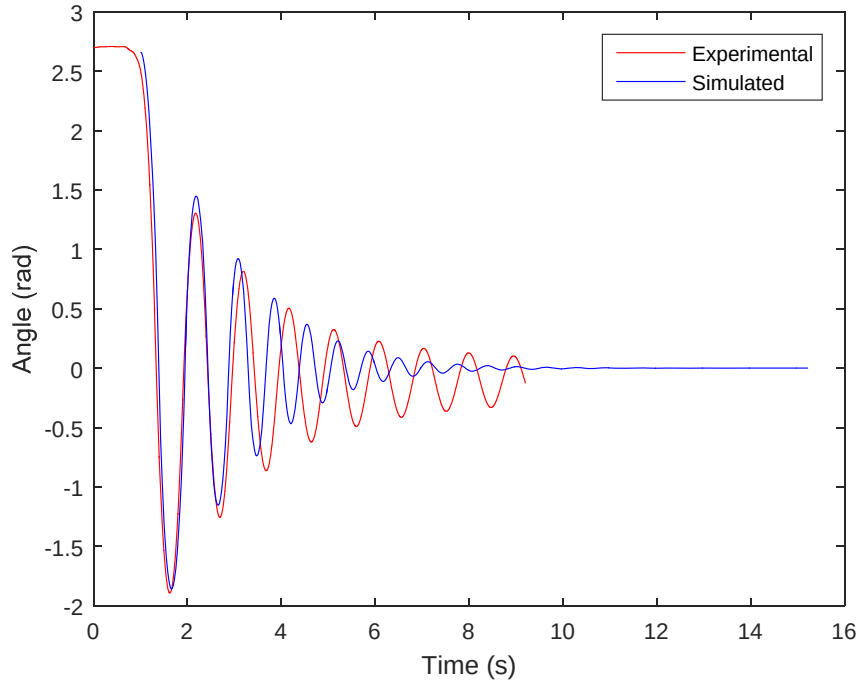

Figure 8. Experimental and Simulated Pendulum Motion with No Controller

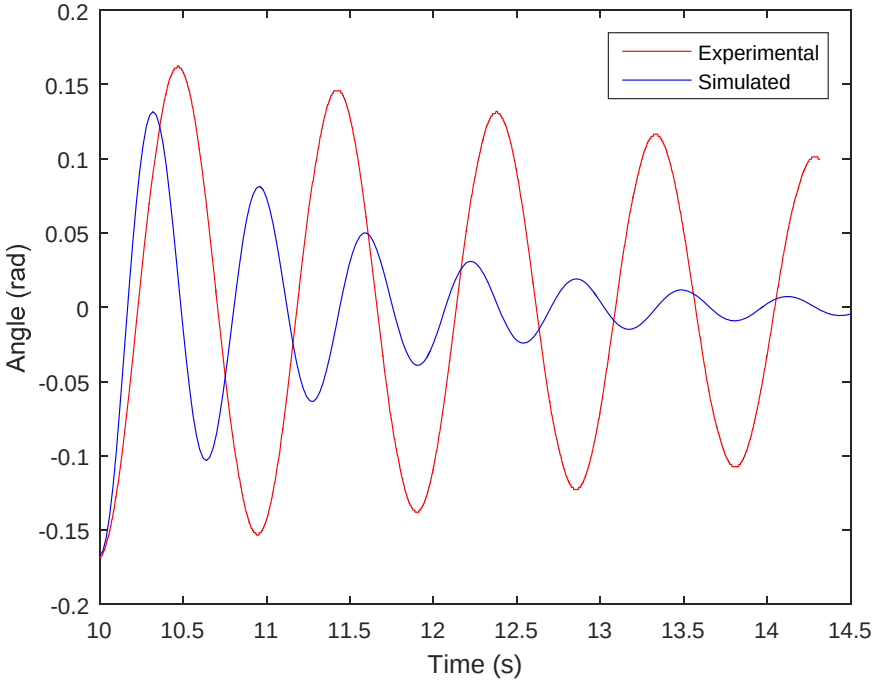

Figure 9. Experimental and Simulated Pendulum with No Control with a Small Initial Angle

As seen in both figures, the period of oscillation of the simulation is faster than that of the actual rotary pendulum. Additionally, simulation damps off faster than the experimental data. The experimental and simulated data more closely match each other when the initial angle is large. This indicates some nonlinearity not modeled in the system. The large discrepancy between the simulation and experimental motion indicates that system is not modeled correctly. Because feedback linearization is based on the model of the system, it is critical that the model is accurate. The system model was examined more closely by looking at another source due to some ambiguity in the manual's model derivation. In [18], Cassolato and Prime derive a model for the rotary inverted pendulum using both the Euler-Lagrange method as well as the Newton-Euler method. While their method is similar to that found in the rotary inverted pendulum user manual, they do not make simplifications involving the moments of inertia until the very end. This leads to a very clear and concise model with well-defined parameters. The model derived in [18] is

$$\begin{bmatrix} \ddot{\theta} \\ \ddot{\alpha} \end{bmatrix} = D^{-1}\left(\begin{bmatrix} b_1 + \frac{1}{2}\widehat{J}_2\dot{\alpha}\sin(2\alpha) & \frac{1}{2}\widehat{J}_2\dot{\alpha}\sin(2\alpha) - m_2L_1l_2\sin(\alpha)\dot{\alpha} \\ -\frac{1}{2}\widehat{J}_2\dot{\theta}\sin(2a) & b_2 \end{bmatrix} \begin{bmatrix} \dot{\theta} \\ \dot{\alpha} \end{bmatrix} - \begin{bmatrix} \tau_1 \\ gm_2l_2\sin(\alpha) + \tau_2 \end{bmatrix} \right) \tag{14}$$

where

$$D = \begin{bmatrix} \widehat{J}_0 + \widehat{J}_2 sin^2(\alpha) & m_2L_1l_2\cos(\alpha) \\ m_2L_1l_2\cos(\alpha) & \widehat{J}_2 \end{bmatrix}. \tag{15}$$

The parameters used in Equations (14) and (15) as well as the values for each as given in the QUANSER manual are defined in Table 3.

Table 3. Inverted Pendulum System Parameters. Adapted from [11].

Variable	Description	Value
$\boldsymbol{\theta}$	Angle of the rotary arm from defined zero angle	N/A
$\boldsymbol{a}$	Angle of the pendulum from straight down	N/A
$\boldsymbol{L_1}$	Total length of the rotary arm	0.216 m
$\boldsymbol{l_1}$	Distance of rotary arm pivot point to center of mass	0.0619 m
$\boldsymbol{L_2}$	Total length of the pendulum	0.337 m
$\boldsymbol{l_2}$	Distance of pendulum from pivot point to center of mass	0.156 m
$\boldsymbol{m_1}$	Mass of the rotary arm	0.257 kg
$\boldsymbol{m_2}$	Mass of the pendulum	0.127 kg
$\boldsymbol{b_1}$	Viscous damping coefficient of the rotary arm	-0.0024
$\boldsymbol{b_2}$	Viscous damping coefficient of the pendulum	-0.0024
$\boldsymbol{J_1}$	Moment of inertia of the rotary arm about its center of mass	$9.98 \cdot 10^{-4}$ kg·m^2
$\boldsymbol{J_2}$	Moment of inertia of the pendulum about its center of mass	0.0012 kg·m^2
$\boldsymbol{\widehat{J_1}}$	Moment of inertia of the rotary arm about its pivot point. Using parallel axis theorem: $\widehat{J_1} = J_1 + m_1 {l_1}^2$	0.002 kg·m^2
$\boldsymbol{\widehat{J_2}}$	Moment of inertia of the pendulum about its pivot point. Using the parallel axis theorem: $\widehat{J_2} = J_2 + m_2 {l_2}^2$	0.0043 kg·m^2
$\boldsymbol{\widehat{J_0}}$	Equivalent moment of inertia as seen by the motor of the rotary arm and pendulum together. $\widehat{J_0} = J_1 + m_1 {l_1}^2 + m_2 {L_1}^2$	0.0079 kg·m^2
$\mathbf{g}$	Gravity constant	9.8 m/s^2

In their paper, Cassolato and Prime define the zero angle of the pendulum as straight down. To be consistent with the conventions used in the rest of this thesis, this reference was changed to define the zero angle of the pendulum as straight up by

changing the sign of the gravity term. When using the model given in [18] and the parameters given in the manual, we found that the experimental data still did not fit the simulated data. While the form of the model is likely correct, the given parameters may not be accurate. The simulated and experimental pendulum motion at a large and small initial angle are shown in Figures 10 and 11.

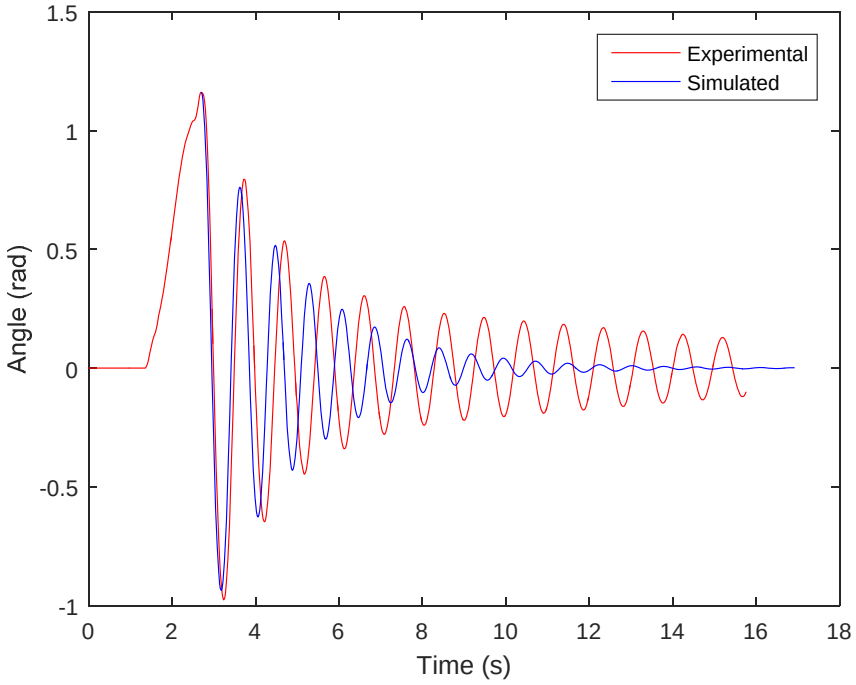

Figure 10. Simulated and Experimental Pendulum Motion with Given Parameters with a Large Initial Angle

The parameters were adjusted until the model fits the experimental data. The parameters that were changed were the length of the pendulum tip to center of mass and the moment of inertia of the rotary arm about its center of mass. The new value of l_2 was 0.1656 m, and the new value of J_1 was 9.98. The experimental data and simulated data with the new parameters starting at a large initial angle are shown in Figure 12. It can be seen from the graph that the simulation seems slightly underdamped at the beginning and overdamped toward the end. Using the same set of adjusted parameters and starting the simulation at a smaller initial angle, we can see that the friction term must be adjusted to

fit the data at a smaller angle. In Figure 13, the simulated response is shown using a smaller initial angle without adjusted friction terms.

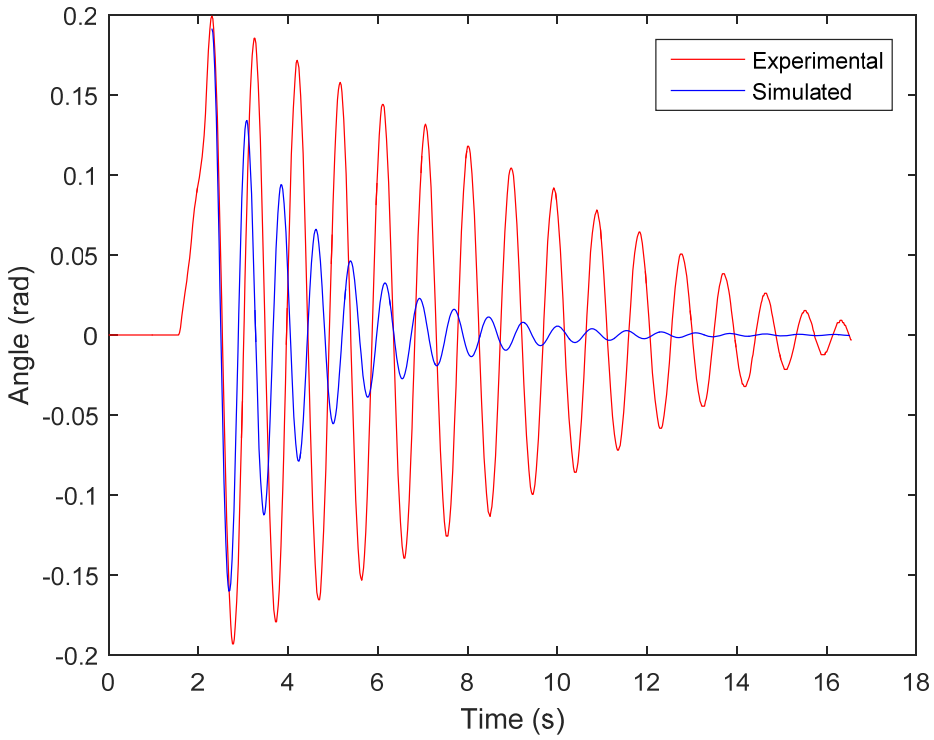

Figure 11. Simulated and Experimental Pendulum Motion with Given Parameters with a Small Initial Angle

When the viscous damping coefficient was adjusted to −0.00085, the model fits the experimental data much better as shown in Figure 14. Toward the end of the simulation, the experimental data does not fit quite as well. Again, this can be attributed to some nonlinearity in the system. Because the pendulum is expected in the neighborhood of the equilibrium point at zero, the friction term that best fit the experimental data at a small initial angle was used.

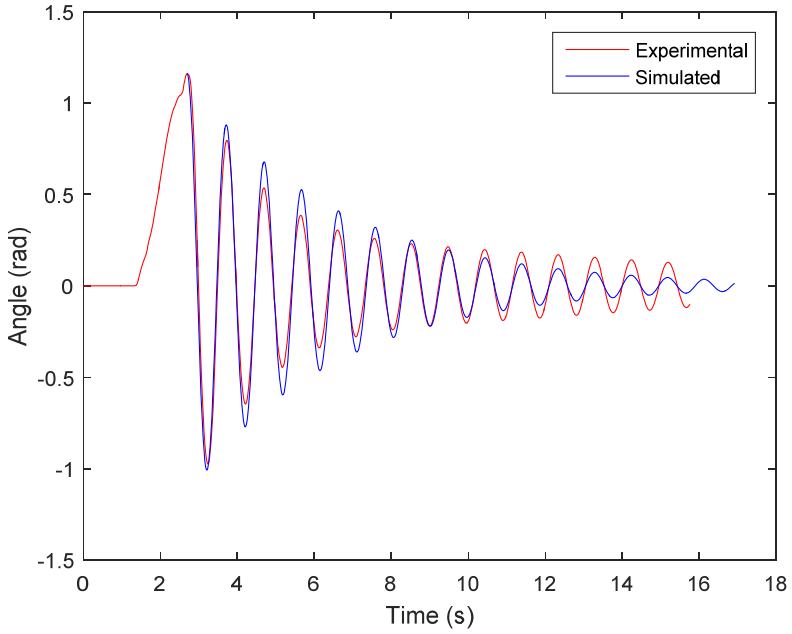

Figure 12. Simulated and Experimental Pendulum Motion with Adjusted Parameters and a Large Initial Angle

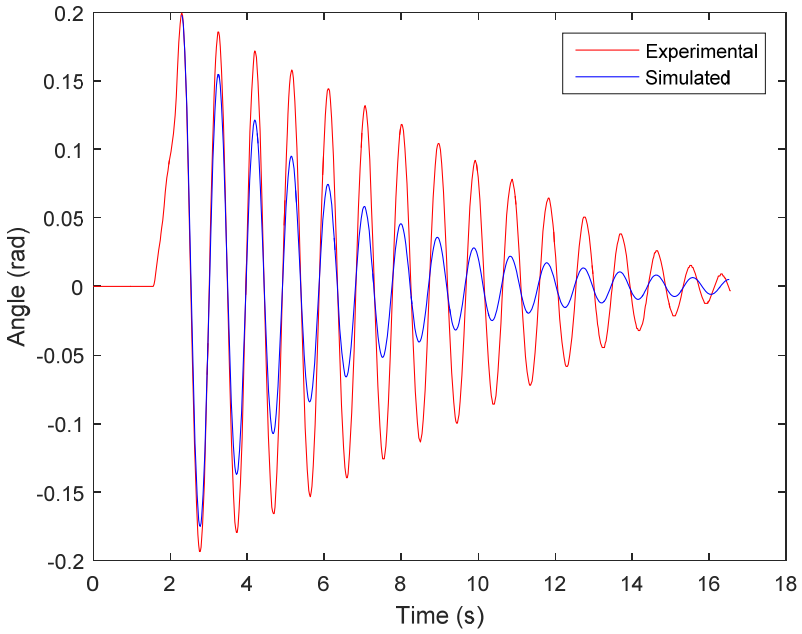

Figure 13. Simulated and Experimental Pendulum Motion with Adjusted Parameters and a Small Initial Angle

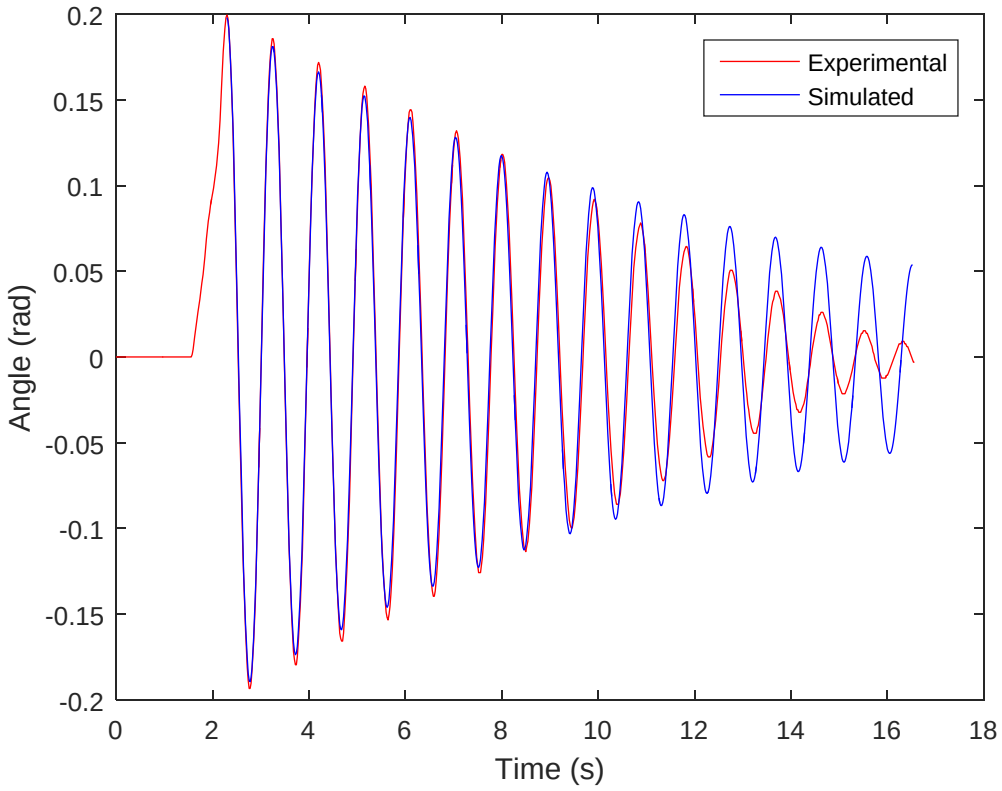

Figure 14. Simulated and Experimental Pendulum Motion with an Adjusted Friction Term and a Small Initial Angle

While the simulated data fits the experimental data well using these new parameters, the new value of J_1 is likely not correct. The parameter was changed by an order of 10^4 to get the results in Figures 12 and 14. This may be related to the DC motor rotor and gear ratio of the SRV02 plant which was not taken into account in this model. The moment of inertia $\hat{J}_0$ should include the moment of inertia of the motor rotor multiplied by the square of the gear ratio. Although the moment of inertia of the motor rotor itself is small, its impact of the pendulum motion may not be negligible due to the gear ratio effect. The values that affect the period of the pendulum are the pendulum length and mass, the rotary arm length and mass, and the moment of inertia of both the pendulum and rotary arm. The pendulum could be easily removed, weighed, and measured because of the way the system was constructed. The published pendulum length was correct within 0.002 m. The published mass was correct within 0.003 kg.

Using the measured length and mass, the moment of inertia was calculated based on the approximation $J \approx \frac{ml^2}{12}$ where J is the moment of inertia. The rotary arm could not be easily removed and measured because of the system construction. It is unclear whether or not the published mass of the rotary arm included the encoder and other wiring on the arm. Additionally, the irregular shape and mass distribution of the rotary arm negates an easy approximation equation being used to calculate the moment of inertia. The additional equipment on the rotary arm was estimated to have a mass of 0.1 kg. The moment of inertia was increased to 2.0×10^{-3}. The viscous damping coefficient was kept at -0.00085. The results of the small angle simulation using these parameters are shown in Figure 15. The parameters are still not exactly right but give a better result than the unadjusted parameters. The remaining discrepancy between the simulation and experimental data could be caused by some unmodeled dynamics such as the interaction of the gearbox with the system.

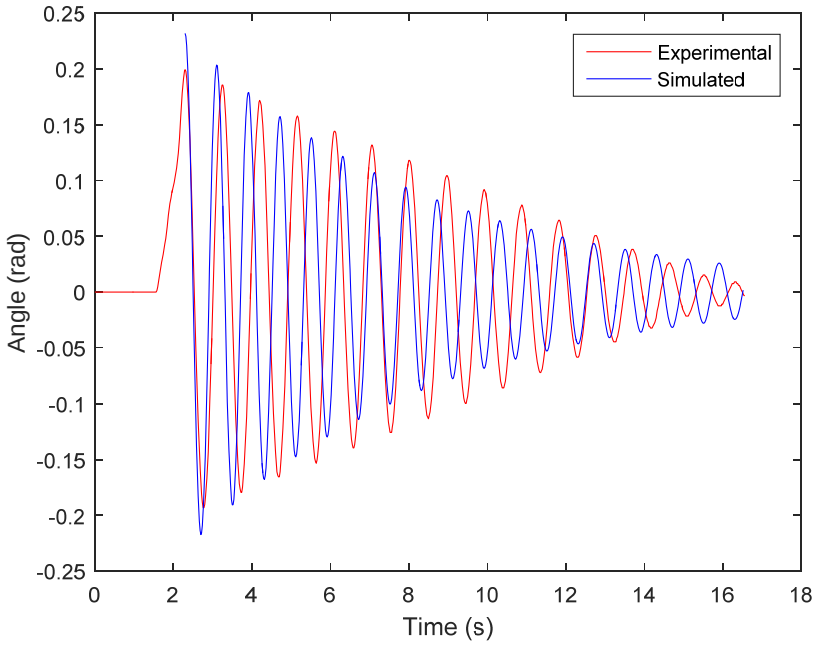

Figure 15. Simulated and Experimental Pendulum Motion Using Moderately Adjusted Parameters

THIS PAGE INTENTIONALLY LEFT BLANK

V. FEEDBACK LINEARIZATION CONTROL

Feedback linearization is a form of control for nonlinear systems in which the nonlinear input effectively cancels out the nonlinearities in the system. A nonlinear system takes the form

$$\begin{aligned} \dot{x} &= f(x) + g(x)u \\ y &= h(x). \end{aligned} \tag{16}$$

Based on the model given in Equations (14) and (15),

$$f(x) = \begin{bmatrix} x_3 \\ x_4 \\ f_3 \\ f_4 \end{bmatrix} \tag{17}$$

where

$$\begin{bmatrix} f_3 \\ f_4 \end{bmatrix} = D^{-1} \left(\begin{bmatrix} b_1 + \frac{1}{2}\widehat{J}_2 x_4 \sin(2x_2) & \frac{1}{2}\widehat{J}_2 x_4 \sin(2x_2) - m_2 L_1 l_2 \sin(x_2) x_4 \\ -\frac{1}{2}\widehat{J}_2 x_3 \sin(2x_2) & b_2 \end{bmatrix} \begin{bmatrix} x_3 \\ x_4 \end{bmatrix} - \begin{bmatrix} 0 \\ g m_2 l_2 \sin(x_2) \end{bmatrix} \right) \tag{18}$$

and

$$g(x) = \begin{bmatrix} 0 \\ 0 \\ g_3 \\ g_4 \end{bmatrix} \tag{19}$$

where

$$\begin{bmatrix} g_3 \\ g_4 \end{bmatrix} = D^{-1} \begin{bmatrix} -1 \\ 0 \end{bmatrix}. \tag{20}$$

In Equations (18) and (20),

$$D = \begin{bmatrix} \widehat{J}_0 + \widehat{J}_2 sin^2(x_2) & m_2 L_1 l_2 \cos(x_2) \\ m_2 L_1 l_2 \cos(x_2) & \widehat{J}_2 \end{bmatrix}. \tag{21}$$

The output of the system is the angle of the pendulum; therefore, the output is given by

$$h(x) = x_2 . \tag{22}$$

The control input $u = Kx$ was used to stabilize the linearized inverted pendulum system in Chapter III. In this chapter, a controller of the form $u = a(x) + b(x)v$ is used.

In order to calculate an appropriate input to linearize the system, the relative degree of the system must be calculated. The relative degree is determined using Lie derivatives. A system has a relative degree r if $L_g L_f^i h(x) = 0$ with $0 \le i \le r-1$ and $L_g L_f^{r-1} h(x) \neq 0$ [19]. The relative Lie derivatives of the rotary inverted pendulum system are

$$L_g h = \frac{\partial h}{\partial x} g = \begin{bmatrix} 0 & 1 & 0 & 0 \end{bmatrix} \begin{bmatrix} 0 \\ 0 \\ g_3 \\ g_4 \end{bmatrix} = 0 , \tag{23}$$

$$L_f h = \frac{\partial h}{\partial x} f = \begin{bmatrix} 0 & 1 & 0 & 0 \end{bmatrix} \begin{bmatrix} x_3 \\ x_4 \\ f_3 \\ f_4 \end{bmatrix} = x_4 , \tag{24}$$

and

$$L_g L_f h = \frac{\partial L_f h}{\partial x} g = \begin{bmatrix} 0 & 0 & 0 & 1 \end{bmatrix} \begin{bmatrix} 0 \\ 0 \\ g_3 \\ g_4 \end{bmatrix} = g_4 \neq 0 . \tag{25}$$

The relative degree of the system is two. The form of a controller for input-output linearization with a relative degree of two is [19]

$$u = \frac{1}{L_g L_f h}\left(-L_f{}^2 h + v\right) . \tag{26}$$

The controller in Equation (26) cancels out the nonlinearities in the system. The linearized system is given by $\ddot{y} = v$. This linear system has two poles at the origin and is unstable. A proportional derivative controller that has the form $v = -2\zeta\omega_n \dot{y} - \omega_n{}^2 y$ is used to stabilize the system. In this equation, the variable ζ is the damping ratio, and the variable ω_n is the natural frequency. These parameters can be changed to affect the performance of the system. In this case, the parameter ω_n was selected to be 4.0, and the damping ratio ζ was selected to be 0.7.

A. SIMULATION

Initially, the controller performance was simulated in Simulink using S-Functions; however, the S-Function block is not compatible with Quanser hardware, so the controller was built using Math Operations. The simulation was run given an initial angle of ten degrees from vertical. A scope of the states throughout the simulation is shown in Figure 16. A graph of the voltage required from the motor is shown in Figure 17.

As can be seen in the simulation, the pendulum angle converges to zero after only about half a second; however, the rotary arm is shown to keep moving at a constant velocity of approximately 1.1 rad/s until the end of the simulation. With friction modeled in the system, the rotary arm should not move at a constant velocity with no input torque. Throughout the simulation, a voltage of 0.6 V is applied throughout the simulation. This continuous motion does not cause problems in the simulation but could in the experimental system.

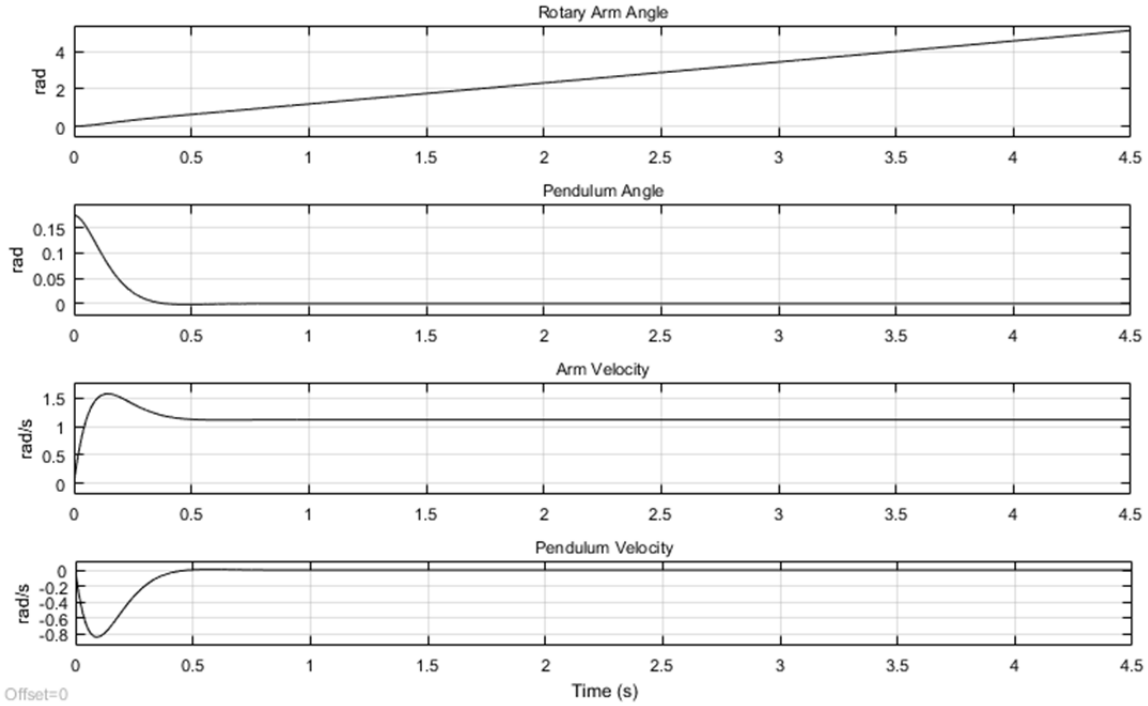

Figure 16. Simulation Output Using Feedback Linearization Control

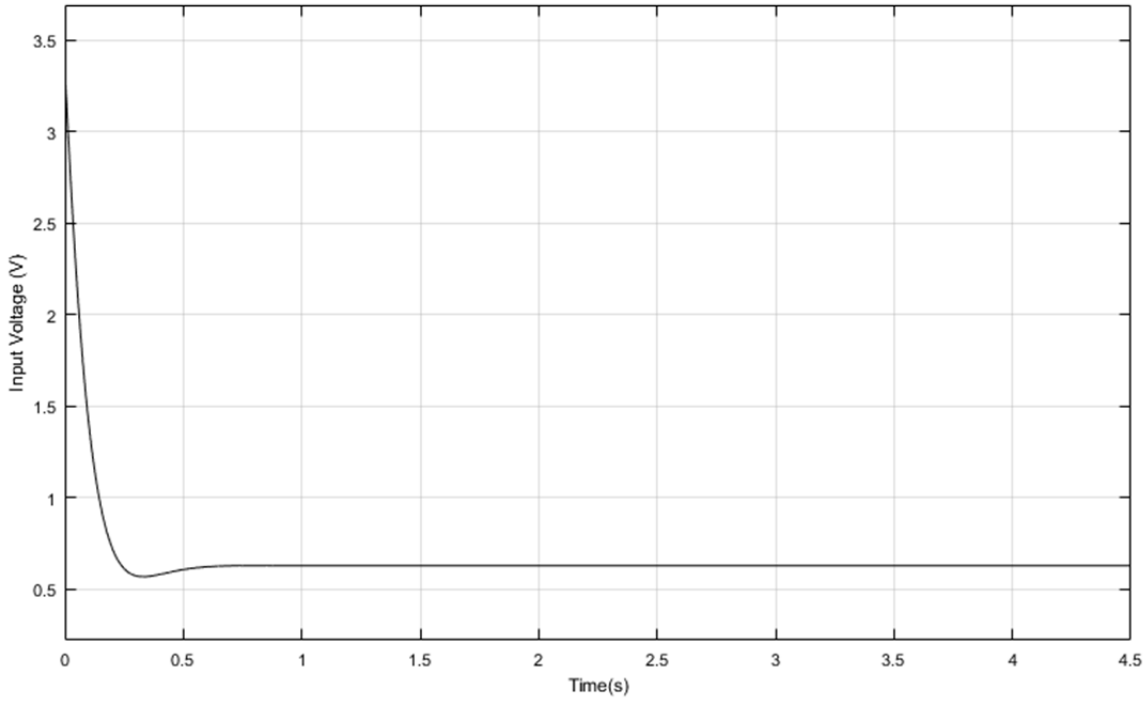

Figure 17. Simulated Voltage Required to Use Feedback Linearization

B. HARDWARE IMPLEMENTATION

When the controller was implemented on the hardware, the pendulum was stabilized to a certain extent. The pendulum was manually brought to the vertical position and then the controller was triggered. The pendulum stayed inverted as the rotary arm revolved around its pivot point in the beginning of the experiment. The rotary arm sped up throughout the trial, which caused the pendulum to fall. Plots of the pendulum angle, rotary arm angle, and input voltage are shown in Figures 18, 19, and 20, respectively. This trial was terminated after 3.5 s when the rotary arm had completed a nearly full revolution. Unlike the simulated results, the rotary arm accelerated throughout the experiment rather than moving at a constant angular velocity. The input voltage in the experiment was also larger than it was in the simulation. Differences between the two can be attributed to limitations of the system, outside disturbances, or errors in the model.

While the simulation output indicated that the feedback linearization controller could be used to successfully control the rotary inverted pendulum system, the experimental results were less successful. The pendulum of the experimental system could be balanced for a few seconds but always fell as the rotary arm moved faster. The simulated and experimental results may be related to unstable zero dynamics of the system. The zero dynamics of the system are analyzed in the next chapter.

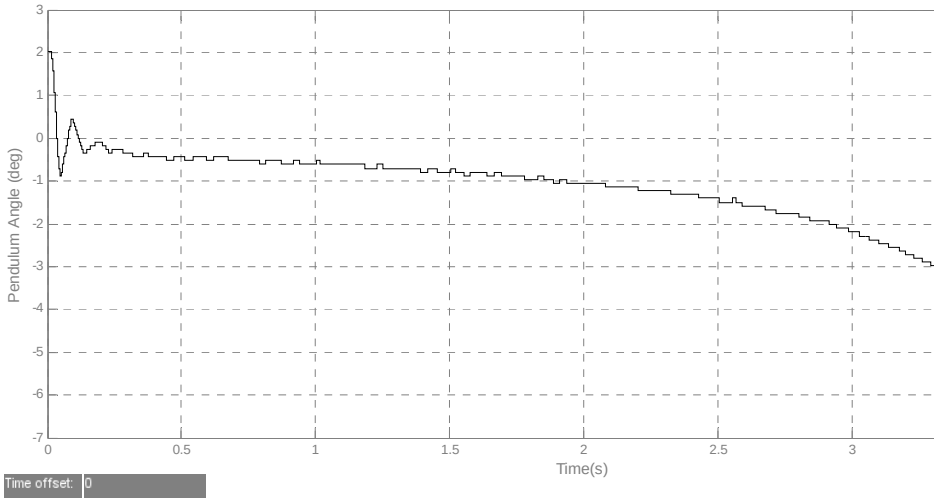

Figure 18. Experimental Pendulum Angle

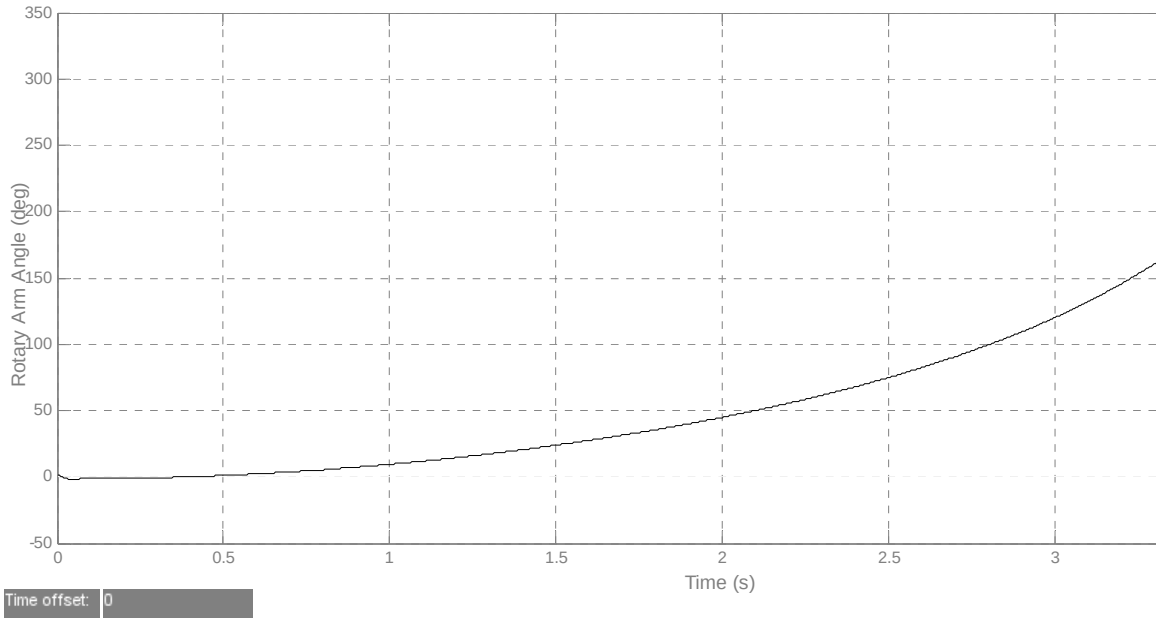

Figure 19. Experimental Angle of the Rotary Arm

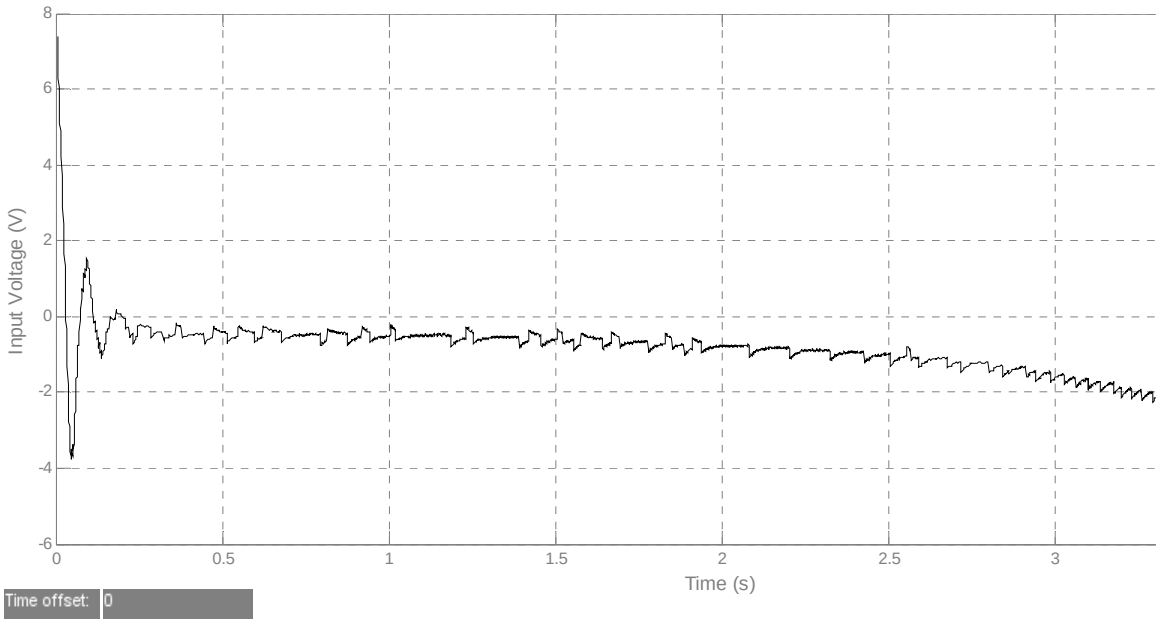

Figure 20. Experimental Output Voltage of Feedback Linearization Controller

VI. ZERO DYNAMICS

The zero dynamics were examined to better understand the behavior of the inverted pendulum system using feedback linearization. Zero dynamics are defined as the systems response when the output is zero. For the rotary pendulum system, the zero dynamics refer to the system response when both the pendulum angle and pendulum angular velocity are zero.

The zero dynamics can be discovered using a state transformation to put the system into the normal form. A state transformation matrix *T(x)* is used to transform the state variables from *x* to *z*. As calculated in Chapter V, the relative degree of the inverted pendulum system is two. The general form for a state transformation for a system of relative degree two is

$$T(x) = \begin{bmatrix} \xi_1 & \xi_2 & \eta_1 & \eta_2 \end{bmatrix}. \tag{27}$$

The first two terms in the transformation matrix relate to the output and its Lie derivatives, while the last two terms η_1 and η_2 relate to the zero dynamics. Typically, the first two terms of *T(x)* are Lie derivatives of ascending degrees of the output along *f(x)*. In the present case of the inverted pendulum system, the expressions for the ξ terms are given by

$$\xi_1 = h = x_2 \tag{28}$$

and

$$\xi_2 = L_f h = x_4. \tag{29}$$

Each η element must have a Lie derivative along the *g* matrix that is equal to zero. That is to say

$$L_g \eta_k = \begin{bmatrix} \frac{\delta \eta_k}{\delta x_1} & \frac{\delta \eta_k}{\delta x_2} & \frac{\delta \eta_k}{\delta x_3} & \frac{\delta \eta_k}{\delta x_4} \end{bmatrix} \begin{bmatrix} 0 \\ 0 \\ g_3 \\ g_4 \end{bmatrix} = 0 \tag{30}$$

for $k = 1, 2$. There are three unique choices for η that satisfy this constraint. The first is $\eta = x_2$. Because this value has already been assigned to ξ_1, it cannot be used. The second value that satisfies this constraint is $\eta = x_1$. Because this value is valid, it is assigned to η_1. The final value can be calculated using

$$\frac{\delta \eta_2}{\delta x_3} g_3 + \frac{\delta \eta_2}{\delta x_4} g_4 = 0 \tag{31}$$

where g_3 and g_4 are defined in Equation (20). Solving Equation (31) results in

$$\eta_2 = \widehat{J}_2 x_4 + \left(m_2 L_1 l_2 \cos\left(x_2 \right) \right) x_3 \ . \tag{32}$$

With all values of *T(x)* defined, the state transformation and inverse state transformations are

$$z = T\left(x \right) = \begin{bmatrix} z_1 & z_2 & z_3 & z_4 \end{bmatrix} = \begin{bmatrix} x_2 & x_4 & x_1 & \widehat{J}_2 x_4 + \left(m_2 L_1 l_2 \cos\left(x_2 \right) \right) x_3 \end{bmatrix} \tag{33}$$

and

$$x = T^{-1}\left(z \right) = \begin{bmatrix} x_1 & x_2 & x_3 & x_4 \end{bmatrix} = \begin{bmatrix} z_3 & z_1 & \dfrac{z_4 - z_2 \widehat{J}_2}{m_2 L_1 l_2 \cos\left(z_1 \right)} & z_2 \end{bmatrix}. \tag{34}$$

The internal dynamics are given by $\dot{\eta}$ as a function of η and ξ where ξ is arbitrary. The zero dynamics are obtained from the internal dynamics when ξ is set to zero. Solving for the internal dynamics, we obtain

$$\dot{\eta}_1 = \dot{x}_1 = x_3 = \frac{z_4 - z_2 \widehat{J}_2}{m_2 L_1 l_2 \cos\left(z_1 \right)} \tag{35}$$

and

$$\dot{\eta}_2 = \frac{d}{dt}\left(\widehat{J}_2 x_4 + \left(m_2 L_1 l_2 \cos\left(x_2 \right) \right) x_3 \right) = \frac{\delta \eta_2}{\delta x} f + \frac{\delta \eta_2}{\delta x} g u \ . \tag{36}$$

In Equation (36), the term $\frac{\delta\eta_2}{\delta x} gu$ equals zero as the state transformation terms were selected to satisfy the constraint set in Equation (30); therefore,

$$\dot{\eta}_2 = \frac{\delta\eta_2}{\delta x} f = -x_3 x_4 m_2 L_1 l_2 \sin(x_2) + m_2 L_1 l_2 \cos(x_2) f_3 + \widehat{J}_2 f_4 \tag{37}$$

where f_3 and f_4 are defined in Equation (18). Equations (35) and (37) can be simplified to

$$\dot{\eta}_1 = \dot{z}_3 = \frac{z_4}{m_2 L_1 l_2} \tag{38}$$

and

$$\dot{\eta}_2 = \dot{z}_4 = 0 \tag{39}$$

when the values represented by the variables ξ_1 and ξ_2 are zero. Based on these equations, the linear system

$$\begin{bmatrix} \dot{z}_3 \\ \dot{z}_4 \end{bmatrix} = \begin{bmatrix} 0 & \frac{1}{m_2 L_1 l_2} \\ 0 & 0 \end{bmatrix} \begin{bmatrix} z_3 \\ z_4 \end{bmatrix} \tag{40}$$

can be written to be examined for stability. The system is second order. Both eigenvalues of the system matrix are zero. A system with two repeated poles at zero is unstable. As shown in Figure 16 of the simulated system response, the rotary arm rotated at a constant velocity until the simulation ended. After examining the zero dynamics, this response makes sense given that z_3 relates to the position of the rotary arm, and the derivative given in Equation (40) is non-zero.

In the next chapter, a new controller that includes terms relating to the position and velocity of the rotary arm is developed in order to stabilize the system response.

THIS PAGE INTENTIONALLY LEFT BLANK

VII. INTUITIVE CONTROLLER

The inverted feedback linearization controller should successfully balance the pendulum, but the rotary arm will continue to spin around at a constant velocity based on the results of the simulations in Chapter V shown in Figure 16. One way to stabilize the position of the rotary arm is to add terms to the linear portion of the controller. The original linear portion of the feedback linearization controller is

$$v = -2\zeta\omega_n \dot{y} - \omega_n{}^2 y \,. \tag{41}$$

In Equation (41), the parameter ζ is the damping ratio, and the parameter ω_n is the natural frequency. The output is the pendulum angle, so in Equation (41) the variable y is the pendulum angle, and the variable $\dot{y}$ is the pendulum angular velocity. Because the controller had no terms that relate to the position or velocity of the rotary arm, the rotary arm moved much more than necessary to balance the inverted pendulum. The new controller had the form

$$v = -2\zeta\omega_n \dot{y} - \omega_n{}^2 y - a\dot{\theta} - b\theta \tag{42}$$

where the variable θ is the rotary arm angle and the variable $\dot{\theta}$ is the angular velocity of the rotary arm. The coefficients *a* and *b* were changed and tested to see how the system responded. Initially, both *a* and *b* were given small values of 0.04. The simulated response is shown in Figure 21. The pendulum oscillates more than it did given the original feedback linearization controller but is still stabilized within two degrees of vertical after two seconds of the simulation. The rotary arm is oscillatory throughout the whole six minutes of simulation, but the oscillations dampen and settle to zero. The first rotary arm oscillation is almost ten radians from the zero positon. Ten radians is almost two full revolutions of the rotary arm, so while the motion settles, there is a significant amount of movement at the beginning of the trial. It is desirable for the rotary arm to be bounded within a smaller arc, so the coefficients *a* and *b* were both increased.

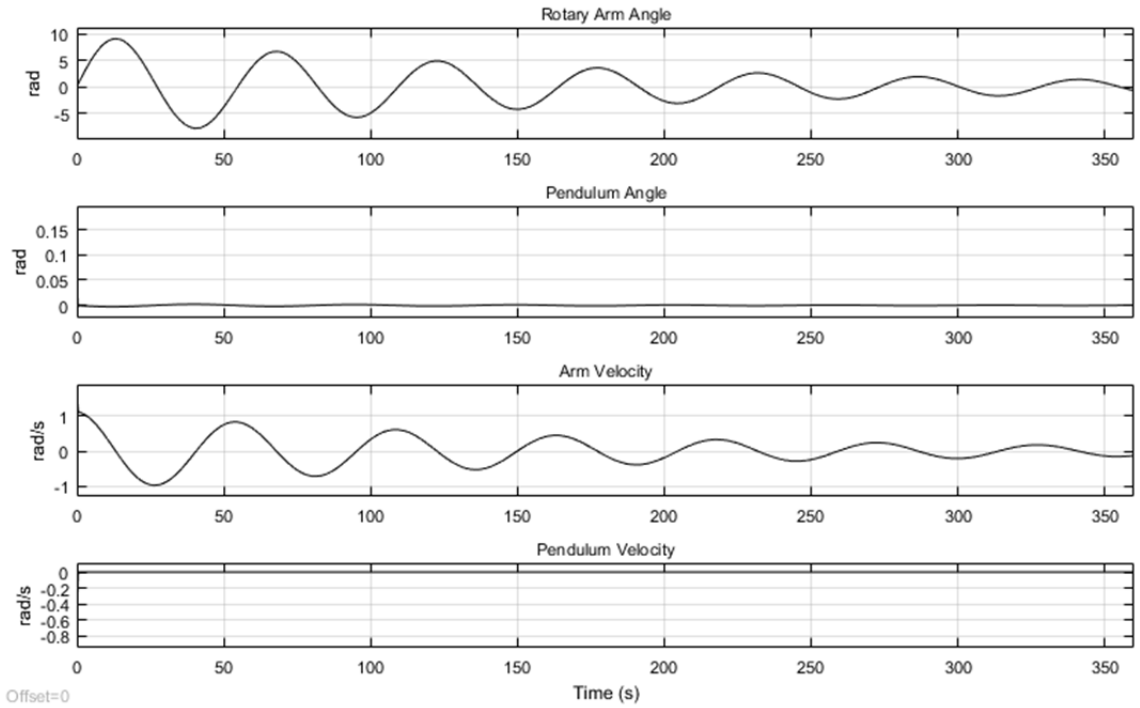

Figure 21. Simulation Output for Coefficients *a* and *b* both Equal to 0.04. The Initial Pendulum Angle was 10 degrees

With coefficients *a* and *b* increased to 1.0, the pendulum response was more oscillatory than it was with smaller *a* and *b* values yet still stable. The rotary arm was bounded within 1.5 radians of the zero position. The arc of the rotary arm is still significant but does not require the rotary arm to spin all the way around. The output of the states is shown in Figure 22. The input voltage is shown in Figure 23. In contrast to the original feedback linearization controller, the input is oscillatory and settles to zero.

The coefficients were increased as much as possible to attempt to reduce the arc of the rotary arm even further. As the coefficients were increased, the system settled faster with smaller oscillations of the rotary arm. When *a* and *b* were increased beyond 12.0, the system response began deteriorating. When *a* and *b* were increased to 14.0, the system became unstable. The simulation response with *a* and *b* equal to 14.0 is shown in Figure 24.

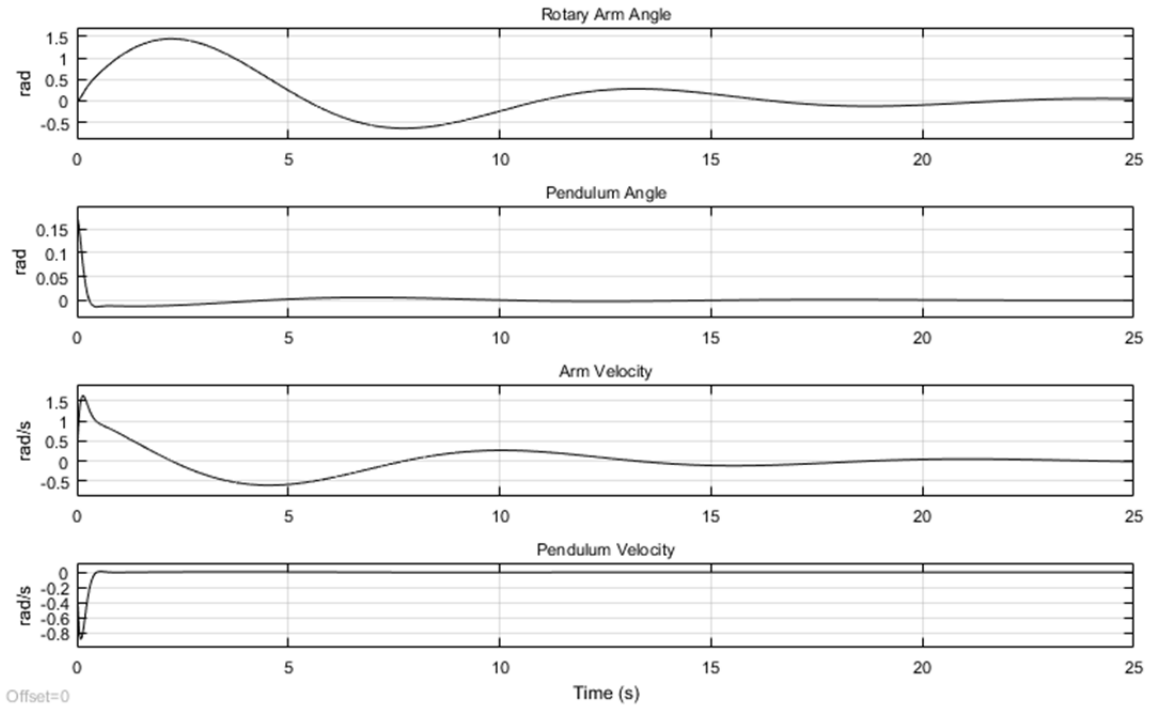

Figure 22. Simulation Output with *a* and *b* Equal to 1.0 and Initial Pendulum Angle of 10 Degrees

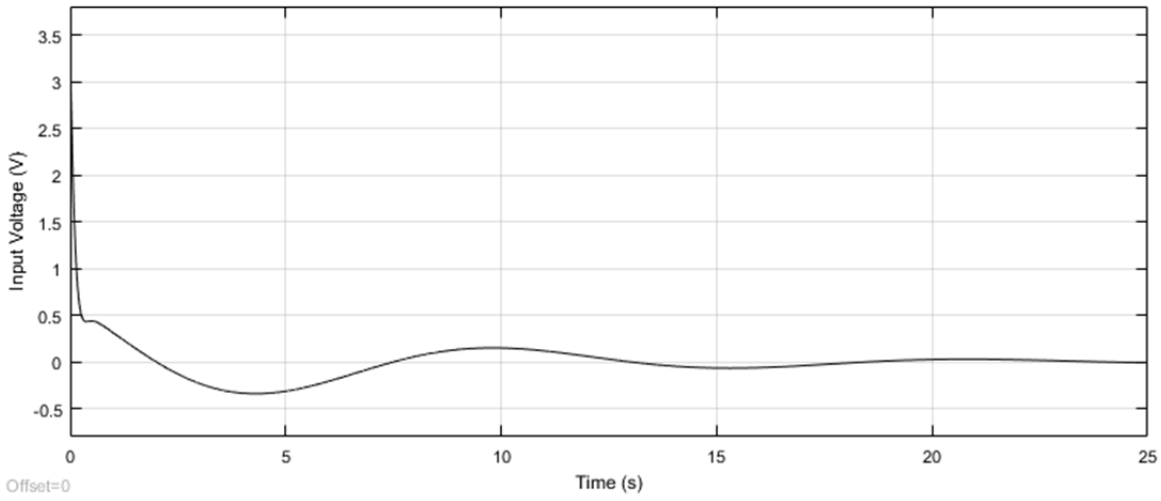

Figure 23. Input Voltage Using the Modified Controller and Coefficient Values of 1.0

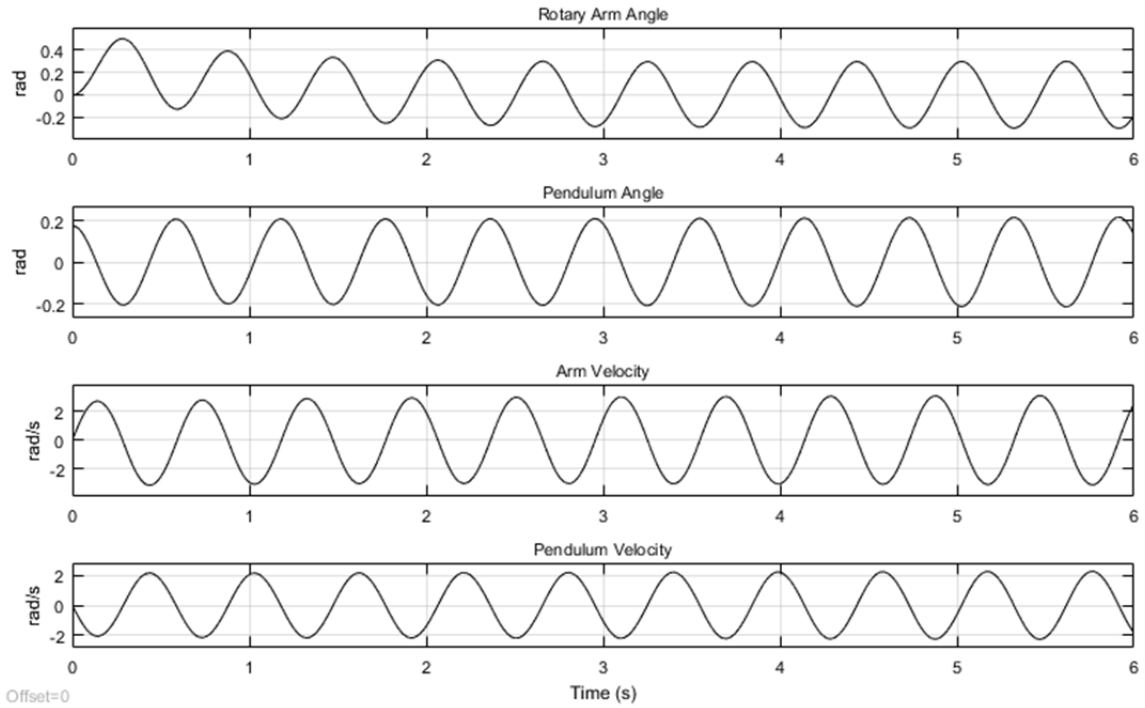

Figure 24. Simulated Output When *a* and *b* are Equal to 14.0 and the Pendulum Has an Initial Angle of 10 Degrees

The simulations confirm that the rotary inverted pendulum can be stabilized by adding terms to the linear portion of the controller. The coefficients of those terms determine the system behavior. If the coefficients are too small, the rotary arm rotates several times before all the states become static. If the coefficients are too large, the system becomes unstable.

VIII. CONCLUSION AND FUTURE WORK

The theory and feasibility of using feedback linearization to control an inverted pendulum system was investigated in this thesis. Initially, linear control was implemented in both simulation and on the experimental system for control familiarization. A linear controller worked well in balancing the pendulum and controlling the position of the rotary arm.

The model of the inverted pendulum system was examined. The model given in the manual had some ambiguous terms and did not fit the experimental pendulum data. A new model based on [18] was developed. Even when the given system parameters were input into the new model, it still did not fit the experimental data. The parameters that could not be easily validated by simply weighing or measuring system parts were changed until the model fit the experimental data. The friction term in the model had to be changed based on the initial angle of the experimental data. Even within one set of data, the model seemed underdamped at the beginning of the trial and overdamped at the end. This indicates that there are nonlinearities in the system that are not in the model. Model parameters that did not cause the simulated pendulum motion to match up with the experimental pendulum motion perfectly were used because they likely represented the system accurately enough.

A feedback linearization controller was designed to balance the inverted pendulum system. The simulations showed that the inverted pendulum was balanced within two seconds, but the rotary arm continued rotating around even after the pendulum was stabilized. After the pendulum was stabilized, a voltage of 0.6 V was constantly applied to the system. When this controller was implemented experimentally, the pendulum was inverted for up to two full revolutions of the rotary arm but always fell as the rotary arm spun faster.

From studying the output of the simulated feedback linearization controller, we can see that the inverted pendulum can be balanced, but the rotary arm continues to move throughout the entire simulation. This is due to the zero dynamics of the system. The

state transformation matrix was calculated, and the zero dynamics were derived. The zero dynamics of the inverted pendulum system were shown to be unstable.

Based on the findings of the unstable zero dynamics, terms were added to the linear portion of the controller that weighed the position and velocity of the rotary arm into the input. In simulation these terms did stabilize the output of the inverted pendulum system. The coefficients a and b in Equation (42) influenced how quickly the system stabilized. These coefficients could be increased up to 14.0 before the position and the velocity of the rotary arm were weighted too heavily, and the inverted pendulum system became unstable.

While feedback linearization control was not proven to work experimentally on a rotary inverted pendulum system, the simulation and theory showed success. The parameters that were changed in order to make the model match experimental data may be different than the actual physical parameters of the system. Additionally, there may be nonlinearities within the system that are not modeled.

In the future, the rotary inverted pendulum model could be studied more thoroughly to construct a model that is proven to be accurate. In particular, the effective moment of inertia should be investigated in detail. The behavior of the motor rotor, rotary arm, and pendulum should be studied with the effect of the gear ratios properly taken into consideration. Based on this new model, feedback linearization could be tested on the experimental system again, perhaps with more successful experimental results.

LIST OF REFERENCES

[1] M. A. Khanesar and M. A. Shoorehdeli, "Fuzzy sliding mode control of a rotary inverted pendulum," presented at the 5th IEEE International Conference on Computational Cybernetics, Gammarth, Tunisia, 2007.

[2] K. Das and K. K. Paul, "Robust compensation of a cart-inverted pendulum system using a periodic controller: Experimental results," *Automatica*, vol. 47, no. 11. pp. 2543–2547, 2011.

[3] Rotary inverted pendulum FPM-210/211. (2012). Center of Modern Control Techniques and Industrial Informatics. [Online]. Available: http://kyb.fei.tuke.sk/laben/modely/kyv.php. Accessed January 2017.

[4] E. Barbieri, S. Drakunov, and P. D. Grossimon, "Sliding mode control of an inverted pendulum," presented at the Twenty-Eighth Southeastern Symposium on System Theory, Baton Rouge, LA, 1996.

[5] L. B. Prasad, B. Tyahi, and G. H. Om, "Optimal control of nonlinear inverted pendulum system using PID controller and LQR: performance analysis without and with disturbance input," *International Journal of Automation and Computing,* vol. 11, no. 6, pp. 661–670, Dec. 2014.

[6] Q. Wei, W. Dayawansa, and W. Levine, "Nonlinear controller for an inverted pendulum having restricted travel," *Automatica,* vol. 31, no. 6, pp. 841–850, Jun. 1995.

[7] M. A. Khanesar, M. Teshnehlab, and M. A. Shoorehdeli, "Sliding mode control of rotary inverted pendulum," presented at the 15th Mediterranean Conference on Control and Automation, Athens, Greece, 2007.

[8] F. Grasser, A. D'Arrigo, S. Colombi, and A. C. Rufer, "JOE: A mobile, inverted pendulum," *IEEE Transactions on Industrial Electronics,* vol. 49, no. 1, Feb. 2002.

[9] K. Pathak, J. Franch, and S. K. Agrawal, "Velocity and position control of a wheeled inverted pendulum by partial feedback linearization," *IEEE Transactions on Robotics,* vol 21, no. 3, May 2005.

[10] F. Dai, X. Gao, S. Jiang, Y. Liu, and J. Li, "A mulit-DOF two wheeled inverted pendulum robot climbing on a slope," presented at International Conference on Robotics and Biomimetics, Bali, Indonesia, 2014.

[11] *User Manual Inverted Pendulum Experiment,* Quanser Inc., Markham, OH, 2012.

[12] *SRV02 User Manual.* Quanser Inc., Markham, OH, 2011.

[13] S1 Optical Shaft Encoder. (2017) U.S. Digital. [Online]. Available: https://www.usdigital.com/products/encoders/incremental/rotary/shaft/S1

[14] Q2-USB Data Acquisition Device. (2017). Quanser Inc. [Online]. Available: http://www.quanser.com/products/q2-usb

[15] VoltPAQ-X1 Amplifier. (2017). Quanser Inc.[Online]. Available: http://www.quanser.com/products/voltpaq-x4

[16] QUARC Real-Time Control Software. (2017). Quanser Inc. [Online]. Available: http://www.quanser.com/Products/quarc

[17] K. Ogata, *Modern Control Engineering*, Upper Saddle River: Prentice-Hall, 1997.

[18] B. S. Cassolato and Z. Prime, "On the dynamics of the futura pendulum," *Journal of Control Science and Engineering,* 2011.

[19] J.-J. E. Slotline and W. Li, *Applied Nonlinear Control*, Upper Saddle River: Prentice Hall, 1991.

INITIAL DISTRIBUTION LIST

1. Defense Technical Information Center
   Ft. Belvoir, Virginia

2. Dudley Knox Library
   Naval Postgraduate School
   Monterey, California